Applied Geography 99 (2018) 120–132

Contents lists available at ScienceDirect

Applied Geography

journal homepage: www.elsevier.com/locate/apgeog

Estimating forest canopy cover dynamics in Valles Caldera National Preserve, New Mexico, using LiDAR and Landsat data

Kamal Humagain[a,*], Carlos Portillo-Quintero[a], Robert D. Cox[a], James W. Cain III[b]

[a] Department of Natural Resources Management, Texas Tech University, 2500 Broadway, Lubbock, TX 79409, USA
[b] U.S. Geological Survey, New Mexico Cooperative Fish and Wildlife Research Unit, Department of Fish, Wildlife and Conservation Ecology, New Mexico State University, 2980 S. Espina, Knox Hall 132, Las Cruces, NM 88003, USA

ARTICLE INFO

Keywords:
LiDAR
Landsat
Percent canopy cover
Restoration
Wildfire

ABSTRACT

Increasing tree canopy cover has led to increasing wildfire activity in conifer dominated areas of the southwestern United States. Estimating historical changes in the spatial distribution of tree canopy cover can provide further insights into the dynamics of forest and fuel conditions in these landscapes and help prioritize areas for restoration to mitigate wildfire risks and restore biological functioning. In this study, we explored the relationship between LiDAR derived canopy cover data and Landsat reflectance values, and derived a model to estimate percent canopy cover (PCC) on historical Landsat data from 1987 to 2015 for the Valles Caldera National Preserve (VCNP), located in the southwest Jemez Mountains of New Mexico. We developed a regression model between LiDAR generated canopy cover collected in June 2010 and Landsat Thematic Mapper (TM) reflectance values (bands 1–7 except band 6) and vegetation indices collected for the same date. About 5% (17,000) of the total LiDAR points (329,102) were used as training points and a separate, non-overlapping set of 17,000 points as test points to validate the regression model. A simple linear model with the red band (band 3; $R^2 = 0.70$) was selected as the best model to predict PCC in the rest of the images for 1987–2015. In general, we found a strong consistency between the spatial dynamics of modelled tree canopy cover based on historical Landsat data, wildfire events and forest management practices that occurred during the same period. Results showed that about 11% of the study area experienced an increase in PCC for the period of 1987–2015 while 41% of the study area experienced a reduction in PCC during the same time period, mostly in the areas which were affected by stand replacing wildfires in 2011 and 2013. The results indicate an overall increase in medium and high canopy cover classes in specific regions of the study area, which could lead to hazardous wildfires such as those in 2011 and 2013. In the context of ongoing ecological restoration of these montane forests, predicted PCC of contemporary forests could help local managers to identify the areas in the need of immediate restoration efforts by focusing management practices on the areas with closed canopy.

1. Introduction

The structure of conifer dominated forests in the southwestern United States was maintained predominantly by fires, insects, and herbivory (mostly by wild ungulates) before Euro-American settlement (Battaglia & Shepperd, 2007). After settlement, management practices such as fire suppression, grazing, and logging, combined with changes in climatic patterns, significantly altered structural and functional patterns in these forests (Covington & Moore, 1994; Moore, Huffman, Fulé, Covington, & Crouse, 2004). Consequently, southwestern forests are currently thought to have higher tree densities, greater canopy cover and lower understory diversity compared to their pre-settlement conditions (Allen et al., 2002; Covington & Moore, 1994; Covington et al., 1997; Reynolds et al., 2013, pp. 1–76). In addition, these forests have become more susceptible to wildfires due to increases in crown closure (Battaglia & Shepperd, 2007). Estimating the spatial distribution of tree canopy cover provides an insight into current forest and fuel conditions in these landscapes and further assists in prioritizing areas for restoration to mitigate wildfire risks and restore biological functioning (Mutlu, Popescu, Stripling, & Spencer, 2008; Stephens, Collins, & Roller, 2012).

The use of remote sensing is considered a reliable method for measuring or modeling forest parameters at landscape and regional scales. Sensors on both satellite and aircraft are able to measure energy patterns reflected from forest ecosystems, and analysts then use multiple techniques to create spatial models of forest parameters or processes based on corresponding energy-forest interactions (Ahmed, Franklin, Wulder, & White, 2015). Light

* Corresponding author. Current affiliation: Department of Geology, The State University of New York at Potsdam, USA.
E-mail addresses: kamal.humagain@ttu.edu, humagak@potsdam.edu (K. Humagain).

https://doi.org/10.1016/j.apgeog.2018.07.024
Received 25 January 2017; Received in revised form 25 July 2018; Accepted 27 July 2018

detection and ranging (LiDAR) is a widely used active remote sensing technique in forest ecology and has been used since the early 1980s in Central and North America (Aldred and Bonner, 1985; Arp, Griesbach, & Burns, 1982). Most LiDAR systems use the time required for an emitted laser to travel to and from an object as a method of data collection; this time is different for objects with different heights, which helps to determine vertical forest parameters (Lim, Treitz, Wulder, St-Onge, & Flood, 2003). The LiDAR data collection process could be highly accurate (i.e. within few centimeters), depending on surface features of the earth, among other factors (Krabill, Collings, Swift, & Butler, 1980; Pereira & Janssen, 1999). LiDAR predictions are highly accurate for estimating forest parameters (R^2 values as high as 0.94 for stand height, 0.95 for basal area and 0.97 for bole volume of spruce-fir) and could save considerable time and expense when surveying forests (Ahmed et al., 2015; Renslow, Greenfield, & Guay, 2000, p. 19).

Unlike other remote sensing methods, LiDAR data are not affected by shadows and tree self-shading, which enhances its accuracy for many forestry applications including stand density, canopy cover, basal area and biomass (Erdody & Moskal, 2010). In addition, LiDAR contrasts with other remote sensing techniques that mostly provide data on horizontal patterns in forest structure, because vertical distribution of vegetation can also be estimated (Lim et al., 2003). Among several LiDAR applications, ecological examples include terrain modeling with an average accuracy of 22 cm (Mongus & Zalik, 2014; Reutebuch, McGaughey, Andersen, & Carson, 2003), land cover classification with accuracies as high as 98% (Antonarakis, Richards, & Brasington, 2008; Sasaki, Imanishi, Ioki, Morimoto, & Kitada, 2012), and estimating forest parameters with an accuracy up to 97% (Hudak, Evans, & Stuart Smith, 2009; Lim et al., 2003). In particular, tree heights (Gaulton & Malthus, 2010; Suárez, Ontiveros, Smith, & Snape, 2005) and canopy cover (Coops et al., 2007; Korhonen, Korpela, Heiskanen, & Maltamo, 2011; Lovell, Jupp, Culvenor, & Coops, 2003; Smith et al., 2009) have been modelled using LiDAR data in conjunction with ground measurements and passive remote sensing data such as Landsat imagery with accuracies as high as 96%, which has the potential to greatly increase the utility of LiDAR measurements.

The Landsat program is one of the commonly used series of optical sensors in orbit for land cover applications. This global satellite monitoring program has been implemented by NASA since the early 1970s and provides the longest continuous global record of Earth's surface (Jensen, 2007). Landsat images have proven crucial for fulfilling forest inventory objectives, particularly in areas with complex topography where field data collection is limited due to accessibility (Franklin, Hall, Smith, & Gerylo, 2003; Vogelmann, Tolk, & Zhu, 2009). Landsat images have also played a vital role in monitoring dynamic forested landscapes in response to disturbances such as fire, logging, and urbanization as they are acquired at the regular intervals, are freely available and may explain up to 97% variability in forest parameters (Clark & Bobbe, 2006; Franklin et al., 2003). In general, reflectance in Landsat Thematic Mapper (TM) visible and water bands decreases with increasing canopy cover in mixed conifer forests such as those that are dominant in the southwestern US, and this occurs because the absorption of energy by leaf pigments and leaf water content increases as the leaf area and biomass increases (Butera, 1986; Fiorella & Ripple, 1993; Spanner, Pierce, Peterson, & Running, 1990). The near-infrared (NIR) band, on the other hand, has been shown to be unresponsive to changes in canopy cover in conifer forests (Butera, 1986).

Landsat images have been used in conjunction with high resolution LiDAR data for estimating several forest parameters in conifer dominated areas. Some examples include the quantification of volume and biomass of deciduous and pine forests in Virginia with maximum R^2 value of 0.39 for deciduous trees and 0.83 for pine trees (Popescu, Wynne, & Scrivani, 2004), leaf area index estimation in ponderosa pine forests of South Dakota with R^2 values of 0.66 and Idaho with maximum R^2 values of 0.86 (Chen, Vierling, Rowell, & DeFelice, 2004; Jensen, Humes, Vierling, & Hudak, 2008), LiDAR based stand height and crown dimensions in planted conifer trees in central Mississippi and eastern Texas with an accuracy between 0.1 and 0.4 m^2 as compared to ground based measurements (Roberts et al., 2005), tree height and crown diameter in Idaho with an overall accuracy of 95% (Falkowski et al., 2006), basal area and tree density in Idaho with R^2 values 0.92 and 0.88 respectively (Hudak et al., 2006), understory vegetation cover estimation in northeastern California with R^2 values in between 0.70 and 0.80 (Wing et al., 2012), and forest canopy fuels in Washington with R^2 values as high as 0.95 when LiDAR and high resolution aerial infrared imagery combined (Erdody & Moskal, 2010). However, most studies in conifer forests estimated forest parameters for a particular year or season, rather than change in forest structure over time.

Unlike other studies which focused on comparing field data and LiDAR derived parameters or using field data for change detection in the forests, we focused on developing a model using LiDAR data and Landsat data and using the model in a series of images to detect change in percent canopy cover over time. In this context, we explored the predictability of Landsat reflectance to estimate LiDAR generated percent canopy cover and explored tree canopy cover dynamics in conifer dominated mountainous areas in the context of recent wildfires and ongoing restoration efforts. To achieve these goals, we analyzed gradual change in percent canopy cover using LiDAR data and Landsat imagery from 1987 to 2015. We developed regression models to predict LiDAR generated percent canopy cover (PCC) from Landsat reflectance and used the best model to monitor the changes in canopy cover over this period with the aim of evaluating canopy cover change within the study area, determine where those changes were located, and explore the causal factors behind these changes. This provides insight into canopy status of the forest and may assist resource managers with identifying areas in need of restoration. In this work, we evaluate the hypotheses that Landsat TM reflectance is a good predictor of LiDAR derived canopy cover, and disturbance factors such as logging activities and wildfires have influenced canopy cover dynamics in the Valles Caldera National Preserve.

2. Materials and methods

2.1. Study area

The study area encompasses the 35,560 ha Valles Caldera National Preserve (VCNP), located in the Jemez Mountains in northern New Mexico (Fig. 1). The preserve consists of about 10,000 ha of montane grasslands (Coop & Givnish, 2007), which we excluded from the analysis, as the focus of the study was forest canopy cover. Data on grassland areas were obtained from the 1992 National Land Cover Dataset (NLCD) which was based on the Landsat TM image acquired on January 1st, 1988 (Vogelmann et al., 2001). We used land cover data based on 1988 imagery to maintain consistency with the beginning of the analysis and to minimize possible errors due to land cover changes through this time. In our analysis, we defined grassland boundaries based on the 1992 land cover data and removed an inner buffer of 100 m from the boundary to allow the inclusion of marginal areas of transition between forest and montane grasslands (Coop & Givnish, 2007) in our analysis.

2.2. Airborne LiDAR data and preprocessing

The National Center for Airborne Laser Mapping (NCALM) collected airborne LiDAR data between June 28 and July 08, 2010 with an average point density of 10 points per square meter (details in Table 1). This mission was accomplished using a Gemini 06SEN/CON195 system installed on a PA-31, tail number N931SA.

With an average of 10 points per square meter, LiDAR point cloud data consisted of a various number of returns depending on the different vegetation types: the higher the number of layers, the higher the number of returns. A small portion of the LiDAR data is shown in Fig. 2 where it represents the points by its height as compared to the digital ortho photo (Fig. 2a and b). A profile view represents the ground points and low, medium and high vegetation (Fig. 2c).

The Valles Caldera National Preserve management personnel was provided with post-processed LiDAR data by NCALM including a “tree

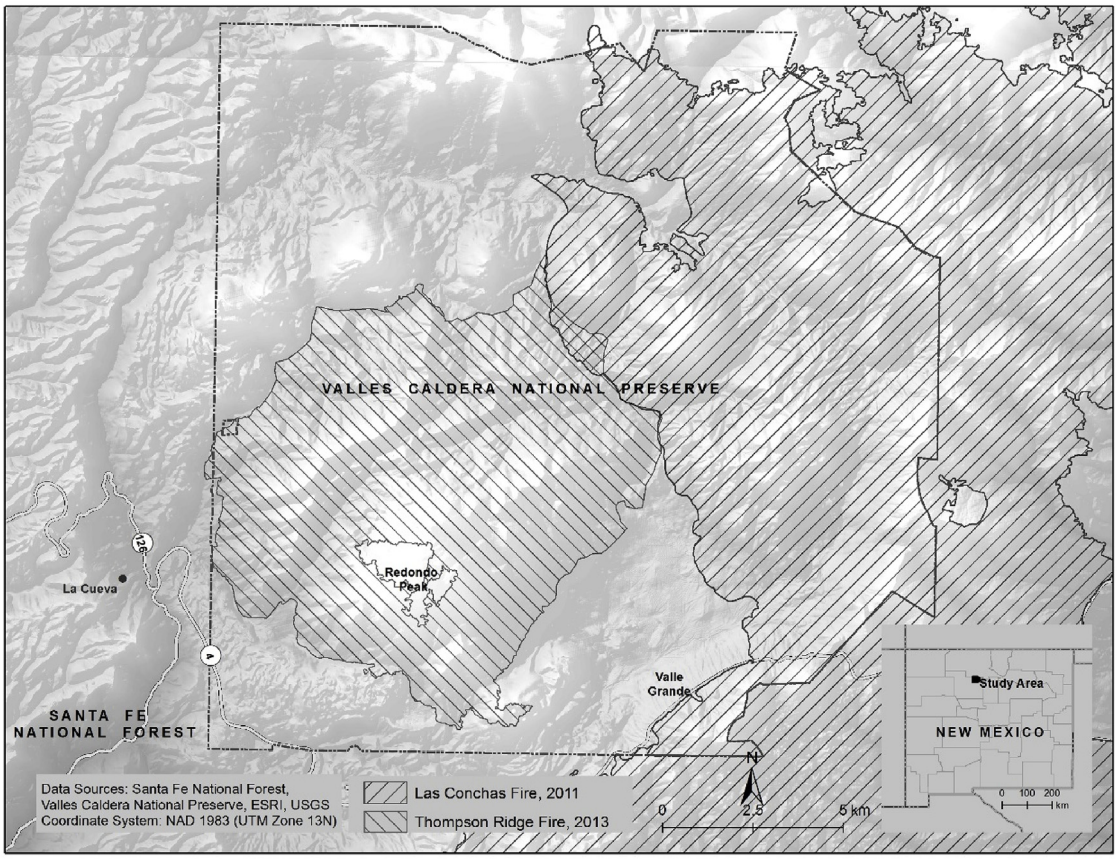

Fig. 1. Study area (Valles Caldera National Preserve).

canopy cover" product at 1 m × 1 m pixel size (minimum mapping unit). These data were provided to the authors upon request. The height cutoff of 1.5 m has previously demonstrated a clear separation between canopy and background, and this is the most commonly used height threshold (McLane, McDermid, & Wulder, 2009). Canopy cover was determined based on the total number of returns above 1.5 m and the total number of points in one-meter pixel (adapted from Nelson, Krabill, & MacLean, 1984):

$$Canopy\ Cover\,(\%) = \frac{Number\ of\ points\ above\ 1.5\ m}{Total\ number\ of\ points} \times 100$$

We used the fishnet tool in ArcGIS 10.5 to create 30 m × 30 m grid corresponding to the Landsat pixels. Using the LiDAR derived percent canopy cover (PCC) at 1 m × 1 m, we used zonal statistics tool in ArcGIS 10.5 to obtain the PCC values at 30 m × 30 m size so that the grids were equivalent to Landsat Pixels. With this tool, using an average statistic, a single LiDAR derived PCC value of 900 pixels was assigned to the corresponding 30 m × 30 m zone. The PCC was then extracted to points so that the points could be used to obtain the reflectance values from Landsat imagery from the same location. Scan angle plays an important role in modeling percent canopy cover in conifers, and the error increases with increasing scan angle (Disney et al., 2010). Korhonen et al. (2011) demonstrated a bias of less than 5% in LiDAR-derived canopy cover in mixed coniferous forests and suggested that groundtruthing may not be required for LiDAR data with low field of view (FOV; 15°). Since the LiDAR FOV in this case was 14° (Guo, 2011), and ground data were not available, we used PCC derived from the LiDAR data without groundtruthing.

Table 1
Parameters of LiDAR data acquisition.

Parameters	Value	Unit
Aircraft velocity	65	meters/second
Flying altitude	600	meters
Field of view (FOV)	± 14	degrees
Pulse rate frequency	100	kilo Hertz
Swath overlap	50	%
Mean ground point density	10.28	points/m^2
Horizontal accuracy	0.25	meters
Vertical Accuracy	0.38	meters

2.3. Landsat data

Landsat TM surface reflectance data were obtained from the United States Geological Survey Landsat archive (http://earthexplorer.usgs.gov/). To minimize the errors due to variability in data acquisition sensors, we focused on Landsat 4/5 TM from 1987 to 2011 and Landsat 8 Operational Land Imager (OLI) thereafter, as the Landsat TM satellite was inactive after 2011. Cloud free Landsat scenes were used to analyze canopy cover change from 1987 to 2015. Landsat images acquired for path 34 and row 35 for 1987-06-22, 1992-07-05, 1999-06-07, 2006-06-10, 2010-06-30 and 2015-06-29 were used in the analysis. Images acquired at the same time of the year (June and early July) were chosen for consistency so that they could be used to best distinguish spectral signatures of the different forest structures (Elmore, Mustard, Manning, & Lobell, 2000). We used TM bands 1 to 7 from 2010 scene (and several calculated indices) except band 6 because of its difference in pixel size during data acquisition (120 m pixels instead of 30 m). In addition, we used Landsat 8 Operational Land Imager (OLI) bands 2 to 7 for 2015. Once the individual bands were stacked into a single file, the image was clipped to the VCNP boundary.

Previous researchers have used six to eight-year intervals to allow the observation of significant land cover changes using Landsat imagery (Drummond et al., 2012; Xian, Homer, & Fry, 2009). For this study, we used four to seven-year intervals, based on data availability. The imagery acquired in 2010-06-30 (path 33, row 35 as path 34, row 35 image had cloud

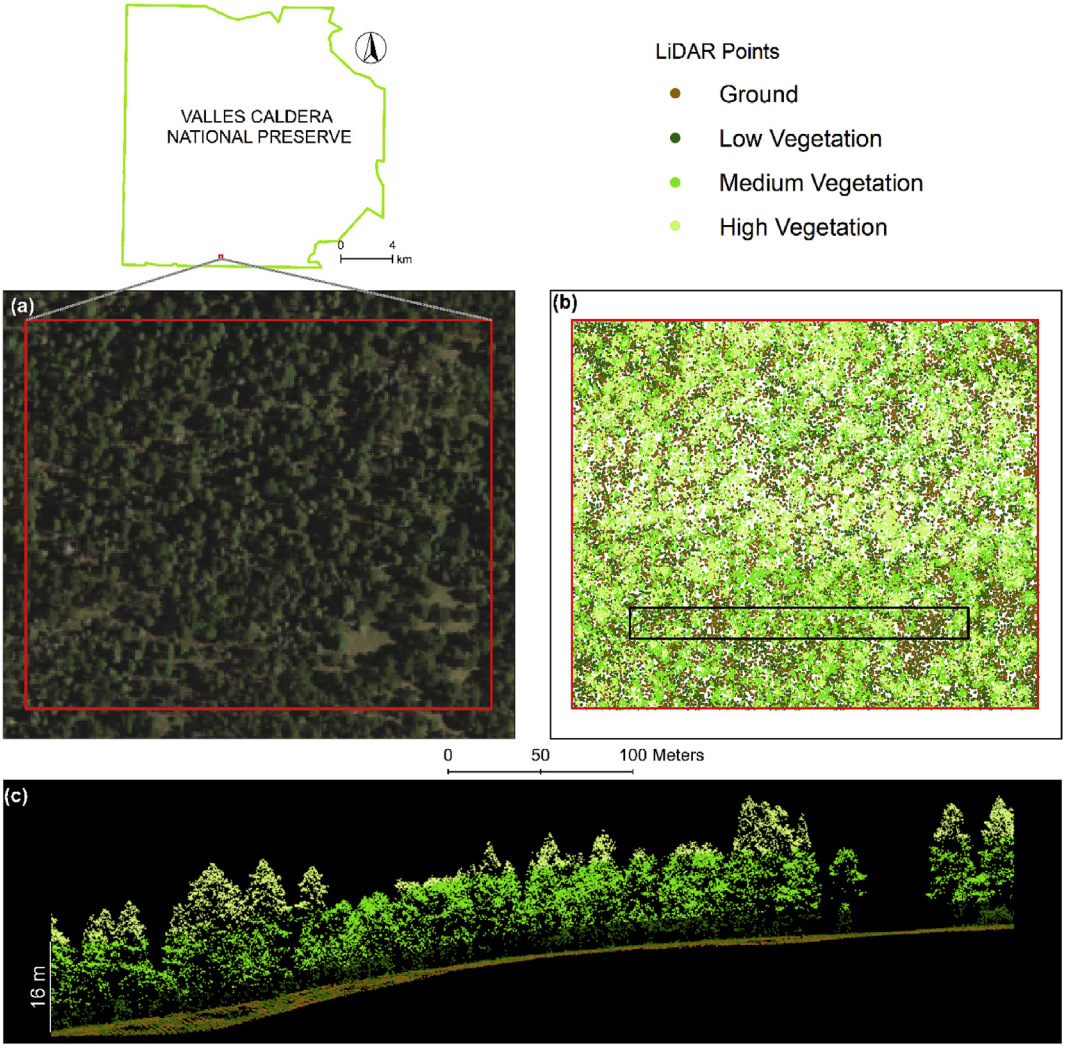

Fig. 2. A sample of LiDAR data in Valles Caldera National Preserve collected in 2010 compared to the National Agricultural Imagery Program (NAIP) digital orthophoto. (a) NAIP scene – 1 m spatial resolution. (b) LiDAR point cloud classified by height – an average of 10 points/m^2. The black box corresponds to the profile view in (c). (c) a profile view of the LiDAR point cloud classified by height.

cover) was used to develop a regression model between LiDAR derived canopy cover and individual bands/vegetation indices. This particular image acquired in 2010 was selected to conform with the time of LiDAR data acquisition so that the error due to seasonality and time was minimized.

2.4. Canopy cover estimation

We randomly selected approximately 5% (i.e. 17,000) of the total 329,102 points as a training dataset to develop the prediction model because considering more than 5% of the points did not improve the model performance. Another non-overlapping set of 17,000 points were randomly selected as a test dataset for model validation. We performed simple linear regression on the training data between LiDAR generated canopy cover and individual explanatory variables (TM band 1 (0.45–0.52 μm), band 2 (0.52–0.60 μm), band 3 (0.63–0.69 μm), band 4 (0.76–0.90 μm), band 5 (1.55–1.75 μm), band 7 (2.08–2.35 μm), simple ratios (SR), difference vegetation index (DVI), several normalized difference indices; Table 2). These vegetation indices were derived from Jordan (1969), Tucker (1979), Clevers (1988), Gao (1996), Lu, Mausel, Brondızio, and Moran (2004), Carreiras, Pereira, and Pereira (2006) and Sivanpillai, Smith, Srinivasan, Messina, and Wu (2006).

In addition, we conducted forward stepwise selection for multiple linear regressions with 6 bands (band 1 to 7 except band 6) and 10 vegetation indices. Among these 16 variables, none of the combinations of two or more variables significantly improved model performance over the individual explanatory variables. We applied accuracy assessment for the test dataset to evaluate the model predictability. Model validation was done based on

Table 2
Formula for vegetation indices for Landsat TM bands.

Indices	Formula*
Simple Ratio based indices	$SR\,1 = \frac{Band\,4}{Band\,3}$, $SR\,2 = \frac{Band\,5}{Band\,3}$, $SR\,3 = \frac{Band\,5}{Band\,4}$, $SR\,4 = \frac{Band\,5}{Band\,7}$
Difference index	$DVI = Band\,4 - Band\,3$
Normalized indices	$NDVI = \frac{Band\,4 - Band\,3}{Band\,4 + Band\,3}$, $ND57 = \frac{Band\,5 - Band\,7}{Band\,5 + Band\,7}$, $ND53 = \frac{Band\,5 - Band\,3}{Band\,5 + band\,3}$, $ND32 = \frac{Band\,3 - Band\,2}{Band\,3 + Band\,3}$, $ARVI = \frac{Band\,4 - (Band\,3 - \lambda(Band\,1 - Band\,3))}{Band\,4 + (Band\,3 - \lambda(Band\,1 - Band\,3))}$ [a]

*SR: Simple Ratio, DVI: Difference Vegetation Index, NDVI: Normalized Difference Vegetation Index, ND57/ND53/ND32: Normalized Difference Indices between bands 5 & 7, 5 & 3 and 3 & 2 respectively, ARVI: Atmospherically Resistant Vegetation Index.

[a] a value of $\lambda = 1$ is recommended for most remote sensing applications by Kaufman and Tanre (1992).

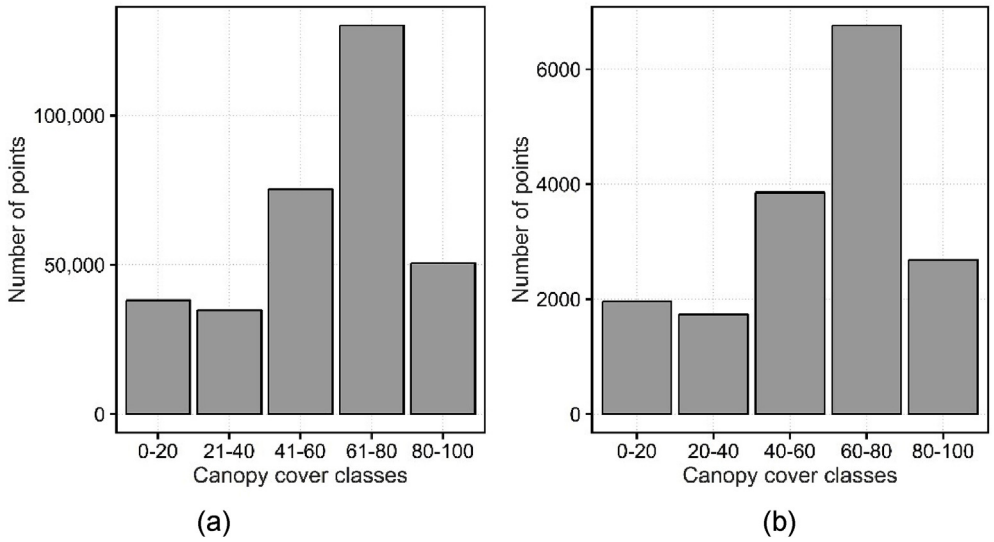

Fig. 3. Percent canopy cover (PCC) derived from LiDAR data collected in 2010. (a) all the points (n = 329,102) and (b) training data (n = 17,000).

the coefficient of determination (R^2), root mean square error (RMSE), mean absolute error (MAE) and mean bias error (MBE):

$$R^2 = 1 - \frac{\sum_{i=1}^{n} (ePCC_{test_i} - PCC_{test_i})^2}{\sum_{i=1}^{n} (ePCC_{test_i} - \overline{PCC_{test}})^2}$$

$$RMSE = \sqrt{\frac{\sum_{i=1}^{n} (ePCC_{test_i} - PCC_{test_i})^2}{n}}$$

$$MAE = \sqrt{\frac{\sum_{i=1}^{n} |ePCC_{test_i} - PCC_{test_i}|}{n}}$$

$$MBE = \frac{\sum_{i=1}^{n} (ePCC_{test_i} - PCC_{test_i})}{n}$$

where n = no. of test points (17,000), $ePCC_{test}$ = estimated percentage canopy cover based on regression model, PCC_{test} = LiDAR derived percentage canopy cover for test data, $\overline{PCC_{test}}$ = Average of the LiDAR derived percentage canopy cover for test data. The best regression model (PCC = 118.49–931.83 Band 3) was used to estimate the canopy cover for all the Landsat scenes for the period of 1987–2015 in ERDAS Imagine.

2.5. Canopy cover change

Based on the prediction by the regression model, percent canopy cover classes were created for each year and the area covered by each class was calculated: 0–20%: no canopy, 21–40%: low canopy; 41–60%: medium canopy; 61–80%: high canopy; 81–100%: closed canopy. To minimize the variation due to Landsat imagery acquired through different years, we used relatively wide canopy cover classes. Consequent change in each class through time was represented on a graph and a map. We used the change detection technique in ArcGIS 10.5 to assess the change in two adjacent years of PCC raster datasets on a pixel by pixel basis for the period of 1987–2015. The difference tool in ArcGIS 10.5 Image Analysis window uses a basic change detection algorithm i.e. subtract function and computes the difference between two raster layers at pixel level. Change maps were prepared for all intervals under consideration and classified as positive change if PCC increased to a higher cover class, neutral if the PCC class remained the same, and negative if the PCC class decreased to a lower class. The burned area extents for 2011 and 2013 were used to compare the spatial distribution of PCC changes and fire affected areas. To evaluate the latest conditions of the forests, we used estimated PCC data for 2015 and analyzed corresponding areas which were: burned in 2011 and 2013, treated (thinning or prescribed fire) before 2015, planned for restoration treatments, or neither treated nor planned for immediate treatments.

3. Results

3.1. Data points

Analogous distribution of the points by PCC classes was observed in the training dataset and complete dataset based on the percent canopy cover (PCC) classes (Fig. 3a and b). Out of the 17,000 points in the training dataset, a majority of the points (40%) represented the high (61–80%) PCC class. A small proportion (15%) of the points were in the closed canopy (81–100%) class and rest of the points (45%) represented the lower canopies (< 60%).

3.2. Bands and vegetation indices

The correlation of individual TM bands and PCC was negative, but most of the vegetation indices showed positive correlation with PCC (Table 3).

Table 3
Relationships between individual bands/vegetation indices computed from the training dataset (n = 17,000) and percent canopy cover.

TM Bands/Vegetation indices[a]	Correlation coefficient (r) with PCC[b]
Band 1 (0.45–0.52 μm)	**−0.81**
Band 2 (0.52–0.60 μm)	**−0.84**
Band 3 (0.63–0.69 μm)	**−0.84**
Band 4 (0.76–0.90 μm)	−0.49
Band 5 (1.55–1.75 μm)	**−0.85**
Band 7 (2.08–2.35 μm)	**−0.83**
SR 1	0.64
SR 2	0.11
SR 3	**−0.77**
SR 4	0.46
DVI	0.04
NDVI	**0.72**
ND57	0.47
ND53	0.12
ND32	−0.63
ARVI	**0.73**

[a] TM: Thematic Mapper, SR: Simple Ratio, DVI: Difference Vegetation Index, NDVI: Normalized Difference Vegetation Index, ND57/ND53/ND32: Normalized Difference Indices between bands 5 & 7, 5 & 3 and 3 & 2 respectively, ARVI: Atmospherically Resistant Vegetation Index.

[b] PCC: Percent Canopy Cover; Top 8 values (correlation coefficient higher than 0.70) are presented in bold face.

Table 4
Performance of the eight tested models, showing coefficients estimates, coefficient of determination (R^2) and adjusted R^2 (n = 17,000).

Model	R^2	Adj R^2	F-statistic	RSE	p-value
PCC^ = 125.69 – 366.88 Band 5	0.73	0.73	463.70	12.76	< 0.001
PCC^ = 118.49 – 931.83 Band 3	**0.70**	**0.70**	**405.90**	**13.38**	**< 0.001**
PCC^ = 137.30 – 1265.52 Band 2	0.70	0.70	405.40	13.39	< 0.001
PCC^ = 112.25 – 455.37 Band 7	0.69	0.69	386.30	13.62	< 0.001
PCC^ = 131.05 – 1664.78 Band 1	0.66	0.66	335.80	14.28	< 0.001
PCC^ = 135.70 – 103.70 SR 3	0.60	0.60	256.90	15.54	< 0.001
PCC^ = −18.21 + 154.87 ARVI	0.54	0.54	199.00	16.72	< 0.001
PCC^ = −56.52 + 195.05 NDVI	0.52	0.52	181.60	17.13	< 0.001

PCC^ refers to estimated percent canopy cover.
SR, Simple Ratio; ARVI, Atmospherically Resistant Vegetation Index; NDVI, Normalized Difference vegetation Index.
RSE, Relative Standard Error.
The model in the bold face was used to predict the canopy cover.

Among all the variables, band 5 (SWIR) showed the strongest linear relationship with PCC (r = −0.85), followed by band 3 (red; r = −0.84) and band 2 (green; r = −0.84). NDVI and ARVI were positively correlated with PCC (r = 0.72 and r = 0.73 respectively). Consequently, among all the individual simple linear regression models, the model with band 5 performed the best (R^2 = 0.73), followed by the model with band 3 (R^2 = 0.70) and band 2 (R^2 = 0.70; Table 4; Fig. 4). However, we selected the model with band 3 as the prediction model instead of band 5 to minimize the effects of moisture content in the forested areas, since band 5 is very sensitive to water (Frazier & Page, 2000; Xu, 2006). In case of Landsat 8, we used band 4 (red) which corresponds to the TM band 3.

Bias associated with the regression model (band 3 as the explanatory variable) was 0.198, mean absolute error was 3.19 and root mean square was 13.29. Predicted vs. LiDAR-derived percent cover for the test data showed a strong correlation (r = 0.84; Fig. 5). The scatterplots revealed that most of the errors were associated with lower canopy cover points.

3.3. Canopy cover change

Large changes occurred in the closed canopy (81–100%) and medium canopy classes (41–60%; Table 5; Fig. 6). There was a loss of closed canopy from 1992 to 1999 (−42.28%) and the loss continued until 2010 (−29.57%). However, closed canopy cover recovered in 2015 (142.09%) as compared to 2010. The lowest canopy cover (0–20%) fluctuated over time and increased exponentially after 2010. For the period of 1987–2015, estimated canopy cover showed a loss of high canopy (−58.42%), and gain in other canopy classes, particularly medium canopy (64.79%) and no canopy cover class (105.49%).

The PCC change map displays an increase in PCC for most of the intervals considered for the analysis (Fig. 7). About 38% of the no canopy cover class experienced an increase to low canopy and about 20% of closed canopy reduced to high canopy in between 1987 and 1992 (Table 6). For the period of 1992–1999, the area experienced overall decrease in the PCC. In particular, between these years, about 43% of closed canopy reduced to high canopy, 30% of high canopy reduced to medium canopy, 28% of medium canopy reduced to low canopy and 62% of low canopy decreased to no canopy. The reduction in PCC continued for the period of 1999–2006 where 55% closed canopy experienced a reduction to high canopy, 20% of medium canopy to low canopy, and 39% of low canopy changed to no canopy (Table 6). Even though about 47% of closed canopy reduced to high canopy in between 2006 and 2010, the study area experienced an increase in PCC in the lower PCC classes where 26% of the no canopy increased to low canopy and 23% low canopy changed to medium canopy. In between 2010 and 2015 even after the large fires of 2011 and 2013, 35.87% and 49.59% of no canopy changed to low canopy and medium canopy respectively, 55.66% of low canopy increased to medium canopy, 56.07% medium canopy changed to high canopy and 26.53% of high canopy changed to closed canopy, however 38.06% of closed canopy reduced to high canopy after 2010.

Most years experienced positive change to next higher class for four to seven year intervals starting in 1987. Considering the entire analysis period (1987–2015), 46.31% of the no canopy changed to low canopy, 49.18% of low canopy increased to medium canopy, and 29.38% of medium canopy changed to high canopy. On the other hand, 26.67% of high canopy reduced to medium canopy and 47.60% of closed canopy decreased to high canopy (Table 6). Most of the increase in canopy occurred along the forest margins and in the lower elevations (Fig. 8). Overall, 11.15% of the study area showed an increase in PCC and 41.47%% of the area showed reduced PCC for the period of 1987–2015. As expected, most of the PCC decrease occurred in the burned areas or treated areas (Fig. 8).

3.4. Current conditions

As of 2015, a majority of the area burned in the wildfires of 2011 and 2013 consisted of high canopy (45.12% and 54.05%, respectively) and medium canopy (25.15% and 23.97%) (Table 7). We found a similar pattern for medium to high canopy in the treated areas (thinning and prescribed burn) as well, though the proportion of high (37.28%) and medium canopy (36.80%) were more similar to each other. Whether the areas were burned or treated, more than 70% of the area consisted of 41%–80% canopy cover. However, more than 79% of the areas which were neither treated nor burned in the most recent wildfires consisted of 61%–100% canopy cover. In particular, a significant proportion of the areas planned for treatment (39.69%) and not treated (30.90%) consisted closed canopy cover.

4. Discussion and conclusion

We observed a strong correlation between PCC and reflectance in Landsat TM visible and SWIR bands in the Valles Caldera National Preserve. Similar results were reported by other researchers while analyzing forest structure in conifer dominated

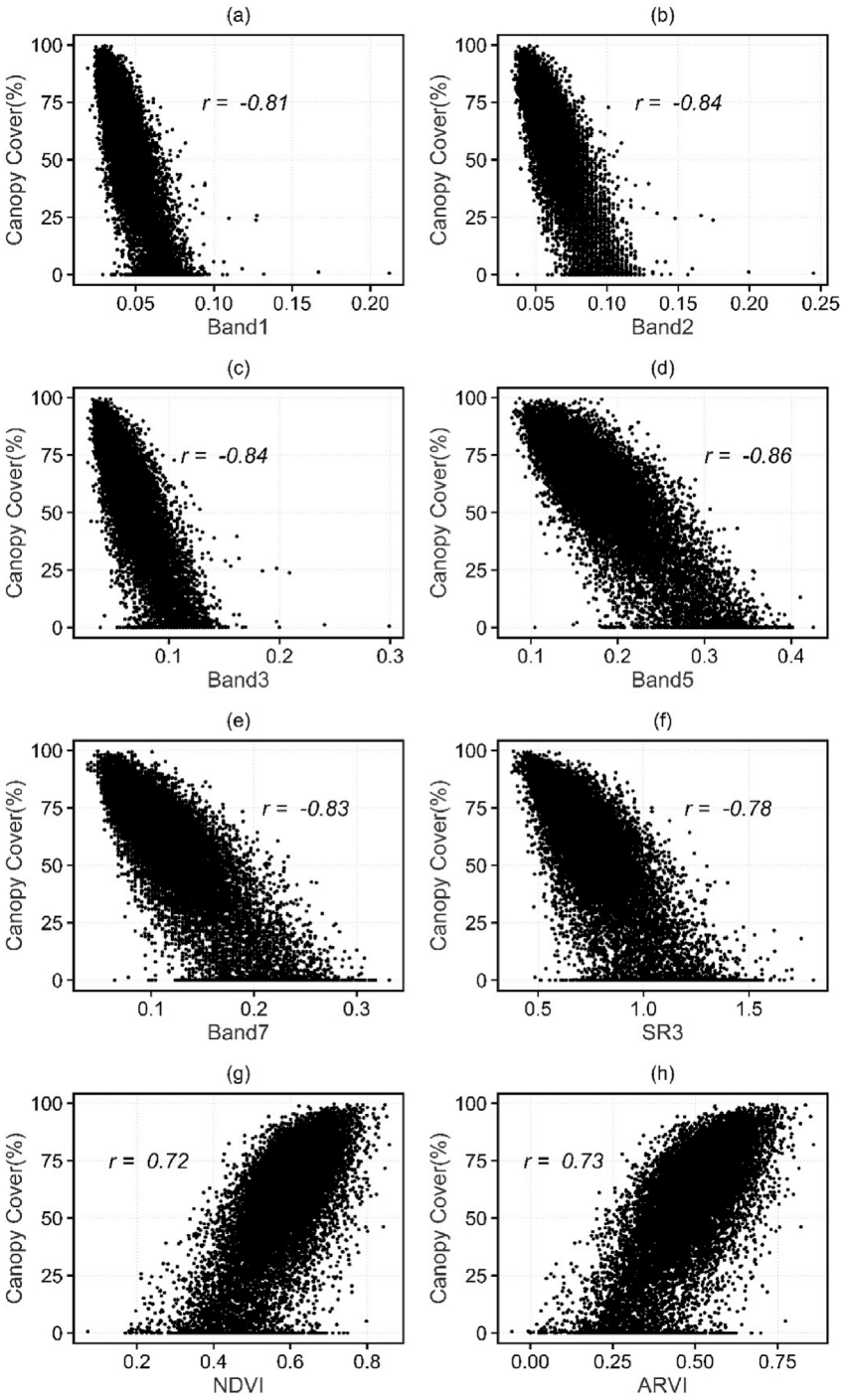

Fig. 4. Scatterplots of percent tree canopy cover (n = 17000) and top 8 highly correlated variables (a) band1; (b) band2; (c) band3; (d) band5; (e) band7; (f) Simple Ratio (SR3); (g) Normalized Difference Vegetation Index (NDVI); (h) Atmospherically Resistant vegetation Index (ARVI).

areas. Canopy cover from spectral mixture analysis showed a strong negative correlation with all the Landsat TM bands (correlation coefficients were −0.68, −0.73, −0.78, −0.74 and −0.74 for bands 1, 2, 3, 5, and 7 respectively) but NIR (r = −0.04) in conifer-dominated forests of Finland (Hadi, Korhonen, Hovi, Rönnholm, & Rautiainen, 2016).

Heiskanen, Rautiainen, Korhonen, Mõttus, and Stenberg (2011) reported a strong negative correlation of leaf area index and

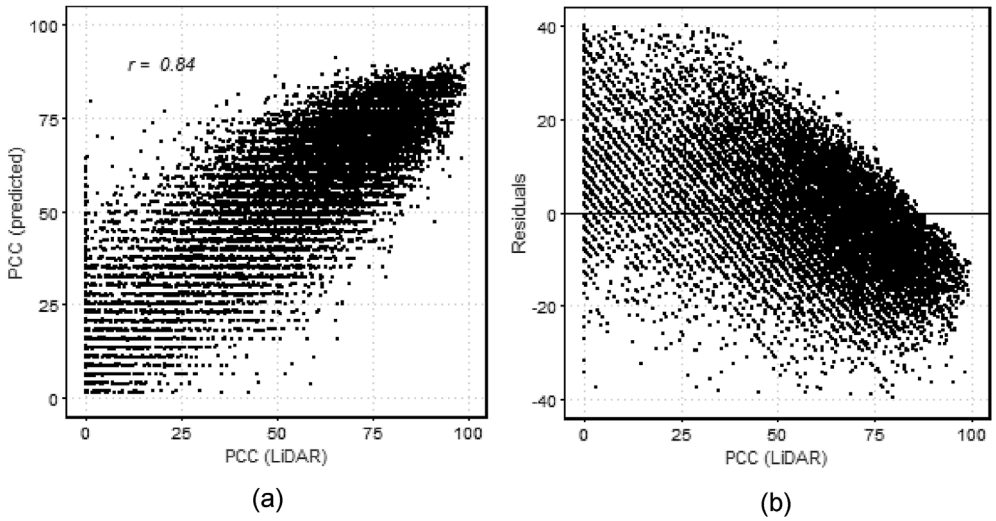

Fig. 5. (a) Scatterplot between LiDAR-derived percent canopy cover (PCC) and predicated PCC for test data (b) Residual plot for test data.

Table 5
Change in percent canopy cover (PCC) classes (1987–2015).

PCC Class	1987 Area (ha)	Change in Area (%)[a]					2015 Area (ha)	1987–2015[b]
		1987–1992	1992–1999	1999–2006	2006–2010	2010–2015		
No Canopy (0–20%)	286.83	**−17.41**	**293.58**	**187.39**	**−19.72**	**−72.60**	589.41	**105.49**
Low Canopy (21–40%)	1,656.45	4.44	**63.14**	6.08	13.43	−28.10	2,441.52	47.39
Medium Canopy (41–60%)	4,883.49	7.70	38.70	−4.72	15.14	0.56	8,047.44	**64.79**
High Canopy (61–80%)	10,837.08	12.22	4.14	11.18	−0.45	−3.19	13,569.30	25.21
Closed Canopy (81–100%)	11,955.42	**−14.42**	−42.28	**−50.62**	**−29.57**	**142.09**	4,971.60	**−58.42**

[a] The values in the bold face represent the top two changes as compared to the previous year.
[b] The values in bold face represent the top three changes during the entire analysis period.

reflectance in red and SWIR bands and a weak negative correlation in NIR band. In addition, Butera (1986) reported a low negative correlation (−0.14) between canopy closure and NIR band based on Thematic Mapper Simulator data while analyzing the conifer forests of Colorado. These studies suggest that NIR does not respond to changes in canopy cover and that the causal factor for such weak

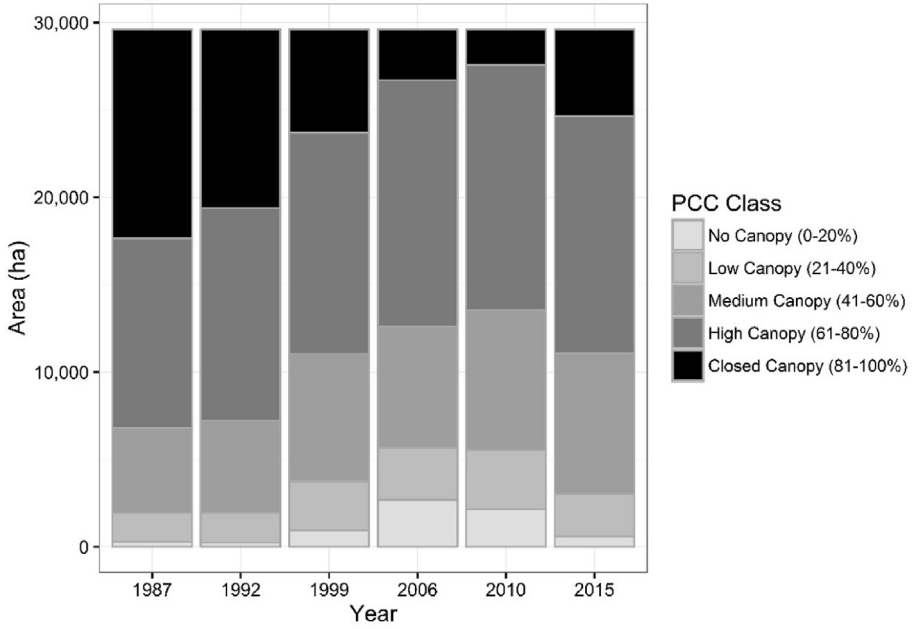

Fig. 6. Percent canopy cover (PCC) classes and the area covered (1987–2015).

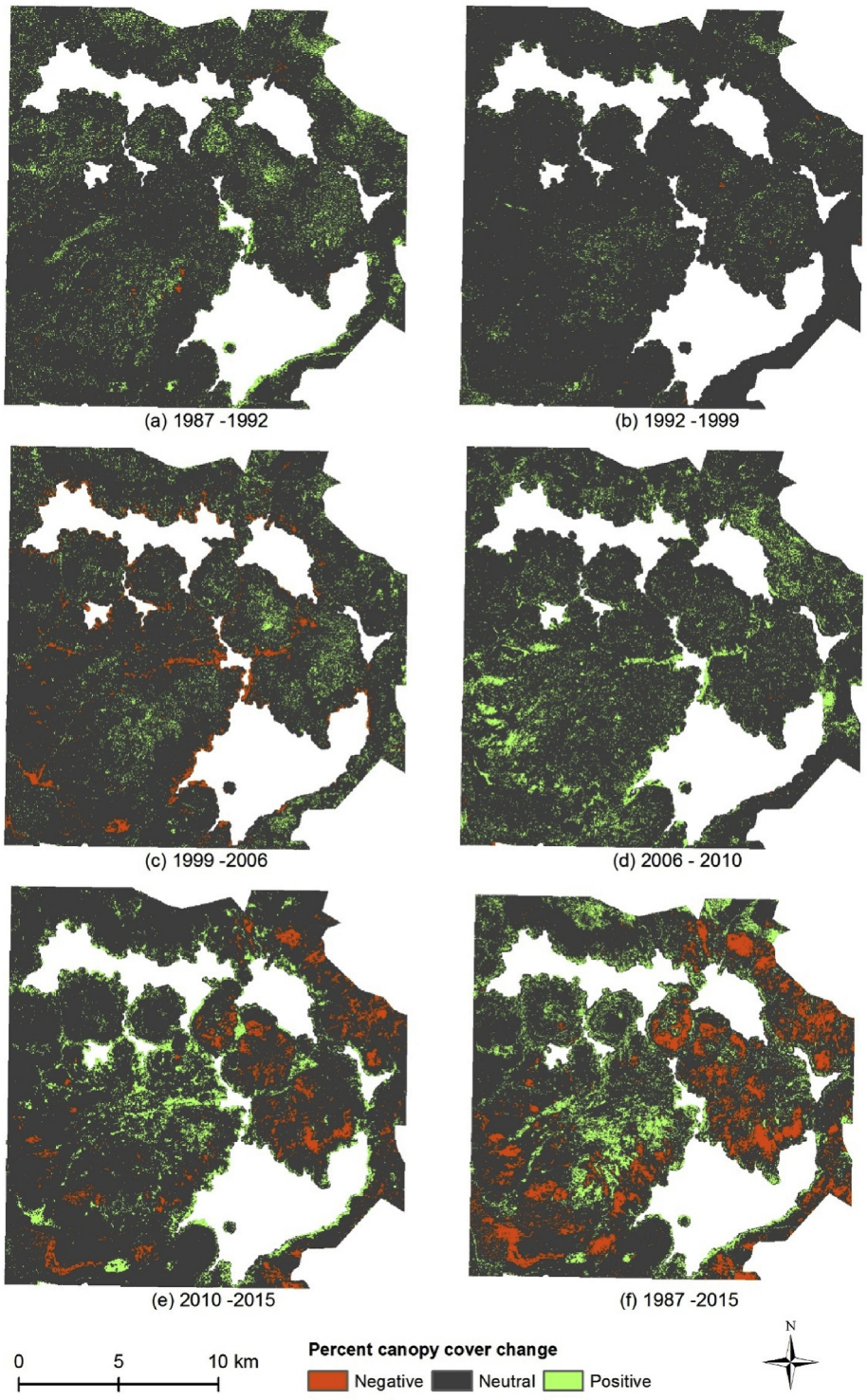

Fig. 7. Percent canopy cover change (1987–2015).

response is the influence of understory vegetation response in conifer forests. Juvenile trees, bare soil, grasses and shrubs in the understory all increase background NIR reflectance in sparse conifer forests. Given that conifer forests allow for higher penetration of sunlight to the understory (in comparison to broadleaf forests), backscattered NIR reflectance readings are a combination

Table 6
Percent change in the percent canopy cover (PCC) classes.

Years	Old PCC class	Area (%)[a]				
		New PCC class				
		0–20%	21–40%	41–60%	61–80%	81–100%
1987–1992	0–20%	*55.95*	**37.97**	5.90	0.19	0.00
	21–40%	4.49	*66.94*	**27.72**	0.85	0.00
	41–60%	0.02	10.10	*72.15*	**17.68**	0.05
	61–80%	0.00	0.15	**11.31**	*81.60*	6.94
	81–100%	0.01	0.02	0.29	**20.41**	*79.27*
1992–1999	0–20%	*89.67*	**10.11**	0.23	0.00	0.00
	21–40%	**61.66**	*18.11*	20.20	0.03	0.00
	41–60%	3.70	**28.89**	*62.75*	4.66	0.00
	61–80%	0.12	1.93	**29.92**	*66.03*	2.00
	81–100%	0.00	0.07	1.68	**42.91**	*55.34*
1999–2006	0–20%	*89.90*	**9.72**	0.37	0.01	0.00
	21–40%	**39.18**	*47.36*	13.15	0.30	0.00
	41–60%	9.22	**19.74**	*60.39*	10.63	0.02
	61–80%	0.48	0.99	**16.99**	*79.32*	2.22
	81–100%	0.03	0.02	0.30	**55.05**	*44.60*
2006–2010	0–20%	*70.85*	**25.71**	3.15	0.27	0.02
	21–40%	8.22	*67.87*	**22.88**	1.00	0.04
	41–60%	0.08	9.62	*75.90*	**14.35**	0.05
	61–80%	0.01	0.04	**13.91**	*82.44*	3.60
	81–100%	0.00	0.00	0.00	**47.15**	*52.84*
2010–2015	0–20%	*7.75*	35.87	**49.59**	6.54	0.26
	21–40%	2.55	*12.11*	**55.66**	29.13	0.55
	41–60%	2.37	7.41	*31.35*	**56.07**	2.80
	61–80%	1.03	4.48	16.80	*51.16*	**26.53**
	81–100%	0.11	1.81	11.07	**38.06**	*48.94*
1987–2015	0–20%	*34.39*	**46.31**	17.70	1.60	0.00
	21–40%	6.03	*40.33*	**49.18**	4.47	0.00
	41–60%	2.28	12.08	*55.73*	**29.38**	0.53
	61–80%	1.75	5.98	**26.47**	*58.73*	7.07
	81–100%	0.75	3.37	13.32	**47.60**	*34.96*

[a] The italicized values represent the percentage of PCC class which remained in the same class. The values in the bold face represent the highest percentage change of a PCC class to a new class.

of canopy and understory characteristics as well. At moderate pixel resolution such as the one provided by Landsat (30 m), the homogenization of NIR reflectance values are greater and therefore, less sensitive to real changes in tree canopy cover occurring in the ground.

We observed a change in PCC for about 52% of the area between 1987 and 2015. In particular, estimated PCC revealed that there was positive change for the first decade which did not significantly increase in the next decade until 2006, but rather displayed a drop in some areas of VCNP. Reduction in PCC (mostly closed canopy) in the 2000s in the VCNP could possibly be explained by continued logging even after the establishment of the preserve (Muldavin & Tonne, 2003, p. 118) and the reduction after 2011 was largely caused by the large fires of 2011 and 2013 (Fig. 8).

We found that PCC generally increased in the mixed conifer forests of the Jemez Mountains of New Mexico, which agrees with several studies in the region (Covington & Moore, 1994; Dieterich, 1983; Fiedler & Keegan, 2003; Fulé, Korb, & Wu, 2009; Kauffman & Martin, 1989; Lydersen & North, 2012; Lydersen, Collins, Knapp, Roller, & Stephens, 2015; Scholl & Taylor, 2010; Stephens et al., 2013; Stevens et al., 2014, 2016). As increasing canopy has increased the risk of stand-replacing wildfires in these conifer forests, this study suggests that fire could play an important role in reducing canopy fuel (Baisan & Swetnam, 1995, pp. 153–156; Cram, Baker, & Boren, 2006; Hayes & Robeson, 2011; Ouzts, Kolb, Huffman, & Meador, 2015; Rogan & Yool, 2001). However, this study does not advocate the need of stand replacing fires to reduce canopy fuel, but we suggest that prescribed fires could help to maintain healthier ecosystems with less canopy and more understory (Arkle & Pilliod, 2010; Huisinga, Laughlin, Fulé, Springer, & McGlone, 2005; Hunter, Iniguez, & Lentile, 2011; Ryan, Knapp, & Varner, 2013). As of 2015, untreated areas and areas planned for treatment showed higher proportion of 61–100% canopy cover as opposed to the treated and burned areas which showed lower proportion of closed canopy and higher proportion of 41–80% canopy cover. As we estimated more than 87% of the untreated areas have high to closed canopy, this study could help managers to identify potential areas for future restoration plans.

Even though this study was restricted within the VCNP boundary, similar drivers that are causing changes in the forested landscape are prevalent in the southwestern montane forests. Unprecedented occurrence of large fire events is one of the major issues in these landscapes due to the departure of the forests from the historical conditions. Ecological restoration plans have been implemented to avoid such tragedy of the forest resources.

This study used cloud-free Landsat imagery acquired around the same months of the years under consideration, yet the response in the electromagnetic spectrum could be different each year. On the other hand, while we acknowledged forest invasion in grasslands (Coop & Givnish, 2007) and included an inner buffer of 100 m to avoid the errors, this portion of grassland might have resulted in overestimation or underestimation when performing change detection. In addition, inaccuracies could also be associated with the conversion of 1 × 1 m pixel PCC to 30 m × 30 m pixels an average in zonal statistics method in ArcGIS 10.5. Even though the accuracy is high with the LiDAR data when estimating percent canopy cover, the ground data can help to improve the results if it is synchronous with the LiDAR data.

This study also demonstrated high accuracy LiDAR data as an effective means of estimating forest parameters (percent canopy cover in this case) in conjunction with Landsat imagery. This method has been utilized by several researchers in the past (Ahmed et al., 2015; Hill & Thomson, 2005; Kane et al., 2010; Pascual, Garcia-Abril, Cohen, & Martin-Fernandez, 2010; Wulder et al., 2009), but we extended the methodology to estimate historical PCC, which has not been accomplished before in these landscapes. In some cases, LiDAR derived forest parameters have proven to be more accurate than conventional field-based inventory techniques (Maltamo, Eerikainen, Pitkanen, Hyyppa, & Vehmas, 2004). In addition, LiDAR derived canopy cover demonstrated the same trend as succession and vegetation height dynamics (Falkowski, Evans, Martinuzzi, Gessler, & Hudak, 2009). However, the utility of LiDAR techniques is limited because, even when they can be more accurate, they are also more expensive, may display irregularities in terms of spatial and temporal aspects (Ahmed et al., 2015), and repeated sampling with LiDAR data is not available for most areas, especially for historic data. In addition, LiDAR data acquisition have been more common in the recent years than in the past and some of the data collected by the government agencies are freely available (e.g. http://opentopography.org/). Therefore, using both LiDAR and Landsat data together, as we demonstrated here, could be a powerful tool to explain forest dynamics over time.

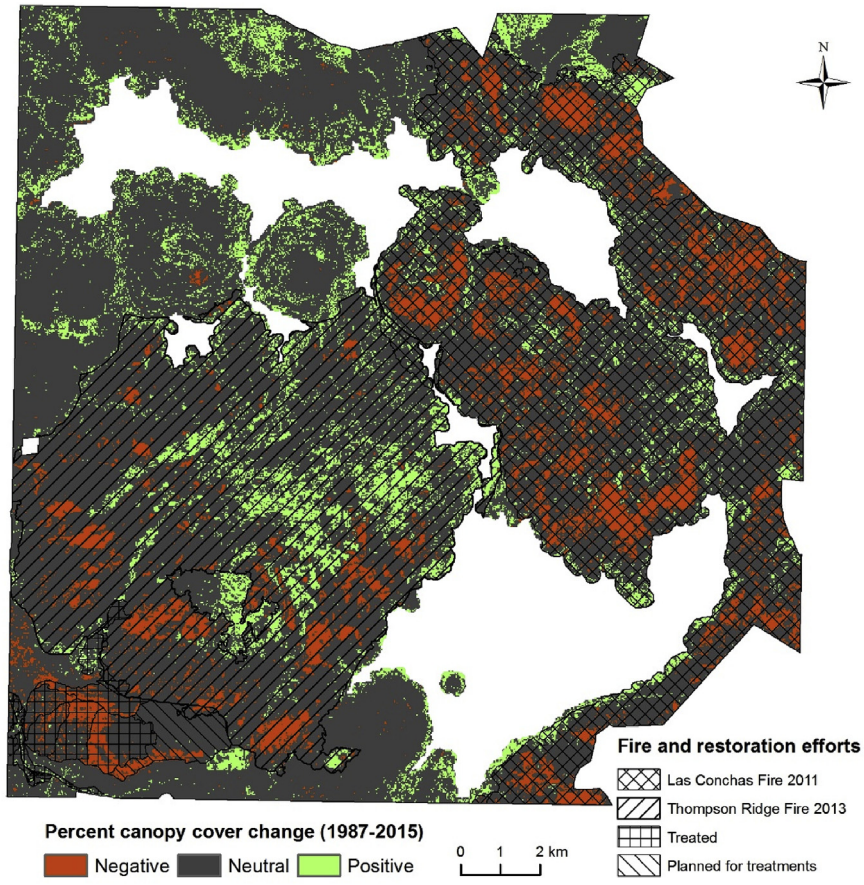

Fig. 8. Percent canopy cover change (1987–2015).

Table 7
Percent canopy cover classes as of 2015.

PCC Class↓	Area (%)[a]				
Area (ha) →	Fire 2011 (10,030.41)	Fire 2013 (9,324.81)	Treated (781.38)	Planned (310.86)	Not Treated (9,364.41)
No Canopy (0–20%)	7.97	1.04	4.75	4.17	0.62
Low Canopy (21–40%)	11.62	5.40	16.06	6.60	4.09
Medium Canopy (41–60%)	**25.15**	**23.97**	**36.80**	9.76	16.99
High Canopy (61–80%)	**45.12**	**54.05**	**37.28**	**39.78**	**47.41**
Closed Canopy (81–100%)	10.14	15.54	5.11	**39.69**	**30.90**

[a] Top two values are in bold faces.

Acknowledgements

We thank Valles Caldera National Preserve (VCNP) for providing the LiDAR data and United States Geological Survey for the Landsat Data. Comments by two anonymous reviewers and K.G. Boykin improved an earlier draft of this manuscript. Any use of trade, firm or product names is for descriptive purposes only and does not imply endorsement by the U.S. Government.

Appendix A. Supplementary data

Supplementary data related to this article can be found at https://doi.org/10.1016/j.apgeog.2018.07.024.

References

Ahmed, O. S., Franklin, S. E., Wulder, M. A., & White, J. C. (2015). Characterizing stand-level forest canopy cover and height using Landsat time series, samples of airborne LiDAR, and the random forest algorithm. *ISPRS Journal of Photogrammetry and Remote Sensing, 101*, 89–101.

Aldred, A. H., & Bonnor, G. M. (1985). *Application of airborne lasers to forest surveys*Petawawa National Forestry Institute, Canadian Forestry Service Information Report PI-X-51.

Allen, C. D., Savage, M., Falk, D. A., Suckling, K. F., Swetnam, T. W., Schulke, T., et al. (2002). Ecological restoration of southwestern ponderosa pine ecosystems: A broad perspective. *Ecological Applications, 12*(5), 1418–1433.

Antonarakis, A. S., Richards, K. S., & Brasington, J. (2008). Object-based land cover classification using airborne LiDAR. *Remote Sensing of Environment, 112*(6), 2988–2998.

Arkle, R. S., & Pilliod, D. S. (2010). Prescribed fires as ecological surrogates for wildfires: A stream and riparian perspective. *Forest Ecology and Management, 259*(5), 893–903.

Arp, H., Griesbach, J., & Burns, J. (1982). Mapping in tropical forests: A new approach using the laser APR. *Photogrammetric Engineering & Remote Sensing, 48*, 91–100.

Baisan, C. H., & Swetnam, T. W. (1995). *Historical fire occurrence in remote mountains of southwestern New Mexico and northern Mexico.* United States Department of Agriculture Forest Service General Technical Report.

Battaglia, M. A., & Shepperd, W. D. (2007). Ponderosa pine, mixed conifer, and spruce-fir forests. *Fire ecology and management of the major ecosystems of southern Utah.US department of agriculture, forest service general technical report RMRS-GTR-202.* Fort Collins, CO: Rocky Mountain Research Station.

Butera, M. K. (1986). A correlation and regression analysis of percent canopy closure

versus TMS spectral response for selected forest sites in the San Juan National Forest, Colorado. *IEEE Transactions on Geoscience and Remote Sensing, 1*, 122–129.
Carreiras, J. M., Pereira, J. M., & Pereira, J. S. (2006). Estimation of tree canopy cover in evergreen oak woodlands using remote sensing. *Forest Ecology and Management, 223*(1), 45–53.
Chen, X., Vierling, L., Rowell, E., & DeFelice, T. (2004). Using LiDAR and effective LAI data to evaluate IKONOS and Landsat 7 ETM+ vegetation cover estimates in a ponderosa pine forest. *Remote Sensing of Environment, 91*(1), 14–26.
Clark, J., & Bobbe, T. (2006). Using remote sensing to map and monitor fire damage in forest ecosystems. In M. A. Wulder, & S. E. Franklin (Eds.). *Understanding forest disturbance and spatial pattern*. Boca Raton, Florida: CRC Press.
Clevers, J. G. P. W. (1988). The derivation of a simplified reflectance model for the estimation of leaf area index. *Remote Sensing of Environment, 25*, 53–70.
Coop, J. D., & Givnish, T. J. (2007). Spatial and temporal patterns of recent forest encroachment in montane grasslands of the Valles Caldera, New Mexico, USA. *Journal of Biogeography, 34*(5), 914–927.
Coops, N. C., Hilker, T., Wulder, M. A., St-Onge, B., Newnham, G., Siggins, A., et al. (2007). Estimating canopy structure of Douglas-fir forest stands from discrete-return LiDAR. *Trees, 21*(3), 295–310.
Covington, W., Fulé, P., Moore, M., Hart, S., Kolb, T., Mast, J., et al. (1997). Restoring ecosystem health in ponderosa pine forests of the southwest. *Journal of Forestry, 95*(4), 23–29.
Covington, W. W., & Moore, M. M. (1994). Post settlement changes in natural fire regimes and forest structure: Ecological restoration of old-growth ponderosa pine forests. *Journal of Sustainable Forestry, 2*(1–2), 153–181.
Cram, D. S., Baker, T. T., & Boren, J. C. (2006). *Wildland fire effects in silviculturally treated vs. untreated stands of New Mexico and Arizona.* Fort Collins, CO: US Department of Agriculture, Forest Service, Rocky Mountain Forest and Range Experiment Station Research Paper RMRS-RP-55.
Dieterich, J. H. (1983). Fire history of southwestern mixed conifer: A case study. *Forest Ecology and Management, 6*(1), 13–31.
Disney, M. I., Kalogirou, V., Lewis, P., Prieto-Blanco, A., Hancock, S., & Pfeifer, M. (2010). Simulating the impact of discrete-return LiDAR system and survey characteristics over young conifer and broadleaf forests. *Remote Sensing of Environment, 114*(7), 1546–1560.
Drummond, M. A., Auch, R. F., Karstensen, K. A., Sayler, K. L., Taylor, J. L., & Loveland, T. R. (2012). Land change variability and human–environment dynamics in the United States Great Plains. *Land Use Policy, 29*(3), 710–723.
Elmore, A. J., Mustard, J. F., Manning, S. J., & Lobell, D. B. (2000). Quantifying vegetation change in semiarid environments: Precision and accuracy of spectral mixture analysis and the normalized difference vegetation index. *Remote Sensing of Environment, 73*(1), 87–102.
Erdody, T. L., & Moskal, L. M. (2010). Fusion of LiDAR and imagery for estimating forest canopy fuels. *Remote Sensing of Environment, 114*(4), 725–737.
Falkowski, M. J., Evans, J. S., Martinuzzi, S., Gessler, P. E., & Hudak, A. T. (2009). Characterizing forest succession with LiDAR data: An evaluation for the Inland Northwest, USA. *Remote Sensing of Environment, 113*, 946–956.
Falkowski, M. J., Smith, A. M., Hudak, A. T., Gessler, P. E., Vierling, L. A., & Crookston, N. L. (2006). Automated estimation of individual conifer tree height and crown diameter via two-dimensional spatial wavelet analysis of LiDAR data. *Canadian Journal of Remote Sensing, 32*(2), 153–161.
Fiedler, C. E., & Keegan, C. E. (2003). Reducing crown fire hazard in fire-adapted forests of New Mexico. *USDA forest service proceedings, RMRS-P: Vol. 29*, (pp. 39–48).
Fiorella, M., & Ripple, W. J. (1993). Analysis of conifer regeneration using Landsat Thematic Mapper data. *Photogrammetric Engineering & Remote Sensing, 59*, 1383–1388.
Franklin, S. E., Hall, R. J., Smith, L., & Gerylo, G. R. (2003). Discrimination of conifer height, age and crown closure classes using Landsat-5 TM imagery in the Canadian Northwest Territories. *International Journal of Remote Sensing, 24*(9), 1823–1834.
Frazier, P. S., & Page, K. J. (2000). Water body detection and delineation with Landsat TM data. *Photogrammetric Engineering & Remote Sensing, 66*(12), 1461–1468.
Fulé, P. Z., Korb, J. E., & Wu, R. (2009). Changes in forest structure of a mixed conifer forest, southwestern Colorado, USA. *Forest Ecology and Management, 258*(7), 1200–1210.
Gao, B. C. (1996). NDWI—A normalized difference water index for remote sensing of vegetation liquid water from space. *Remote Sensing of Environment, 58*(3), 257–266.
Gaulton, R., & Malthus, T. J. (2010). LiDAR mapping of canopy gaps in continuous cover forests: A comparison of canopy height model and point cloud-based techniques. *International Journal of Remote Sensing, 31*(5), 1193–1211.
Guo, Q. (2011). *Critical zone observatory LiDAR mapping project report*Merced, CA: University of California – Merced.
Hadi, Korhonen, L., Hovi, A., Rönnholm, P., & Rautiainen, M. (2016). The accuracy of large-area forest canopy cover estimation using Landsat in boreal region. *International Journal of Applied Earth Observation and Geoinformation, 53*, 118–127.
Hayes, J. J., & Robeson, S. M. (2011). Relationships between fire severity and post-fire landscape pattern following a large mixed-severity fire in the Valle Vidal, New Mexico, USA. *Forest Ecology and Management, 261*(8), 1392–1400.
Heiskanen, J., Rautiainen, M., Korhonen, L., Mõttus, M., & Stenberg, P. (2011). Retrieval of boreal forest LAI using a forest reflectance model and empirical regressions. *International Journal of Applied Earth Observation and Geoinformation, 13*(4), 595–606.
Hill, R. A., & Thomson, A. G. (2005). Mapping woodland species composition and structure using airborne spectral and LiDAR data. *International Journal of Remote Sensing, 26*(17), 3763–3779.
Hudak, A. T., Crookston, N. L., Evans, J. S., Falkowski, M. J., Smith, A. M., Gessler, P. E., et al. (2006). Regression modeling and mapping of coniferous forest basal area and tree density from discrete-return LiDAR and multispectral satellite data. *Canadian Journal of Remote Sensing, 32*(2), 126–138.
Hudak, A. T., Evans, J. S., & Stuart Smith, A. M. (2009). LiDAR utility for natural resource managers. *Remote Sensing, 1*(4), 934–951.
Huisinga, K. D., Laughlin, D. C., Fulé, P. Z., Springer, J. D., & McGlone, C. M. (2005). Effects of an intense prescribed fire on understory vegetation in a mixed conifer forest 1. *Journal of the Torrey Botanical Society, 132*(4), 590–601.
Hunter, M. E., Iniguez, J. M., & Lentile, L. B. (2011). Short-and long-term effects on fuels, forest structure, and wildfire potential from prescribed fire and resource benefit fire in southwestern forests, USA. *Fire Ecology, 7*(3), 108–121.
Jensen, J. R. (2007). *Remote sensing of environment: An earth resource perspective.* New Jersey, USA: Pearson Prentice Hall.
Jensen, J. L., Humes, K. S., Vierling, L. A., & Hudak, A. T. (2008). Discrete return LiDAR-based prediction of leaf area index in two conifer forests. *Remote Sensing of Environment, 112*(10), 3947–3957.
Jordan, C. F. (1969). Derivation of leaf area index from quality of light on the forest floor. *Ecology, 50*, 663–666.
Kane, V. R., Bakker, J. D., McGaughey, R. J., Lutz, J. A., Gersonde, R. F., & Franklin, J. F. (2010). Examining conifer canopy structural complexity across forest ages and elevations with LiDAR data. *Canadian Journal of Forest Research, 40*(4), 774–787.
Kauffman, J. B., & Martin, R. E. (1989). Fire behavior, fuel consumption, and forest-floor changes following prescribed understory fires in Sierra Nevada mixed conifer forests. *Canadian Journal of Forest Research, 19*(4), 455–462.
Kaufman, Y. J., & Tanre, D. (1992). Atmospherically resistant vegetation index (ARVI) for EOS-MODIS. *IEEE Transactions on Geoscience and Remote Sensing, 30*(2), 261–270.
Korhonen, L., Korpela, I., Heiskanen, J., & Maltamo, M. (2011). Airborne discrete-return LiDAR data in the estimation of vertical canopy cover, angular canopy closure and leaf area index. *Remote Sensing of Environment, 115*(4), 1065–1080.
Krabill, W. B., Collings, J. G., Swift, R. N., & Butler, M. L. (1980). *Airborne laser topographic mapping results from initial joint NASA/U.S. Army corps of engineers experiment.* NASA Technical Memorandum 73287, Wallops Flight Center.
Lim, K., Treitz, P., Wulder, M., St-Onge, B., & Flood, M. (2003). LiDAR remote sensing of forest structure. *Progress in Physical Geography, 27*(1), 88–106.
Lovell, J. L., Jupp, D. L., Culvenor, D. S., & Coops, N. C. (2003). Using airborne and ground-based ranging LiDAR to measure canopy structure in Australian forests. *Canadian Journal of Remote Sensing, 29*(5), 607–622.
Lu, D., Mausel, P., Brondızio, E., & Moran, E. (2004). Relationships between forest stand parameters and Landsat TM spectral responses in the Brazilian Amazon Basin. *Forest Ecology and Management, 198*(1), 149–167.
Lydersen, J. M., Collins, B. M., Knapp, E. E., Roller, G. B., & Stephens, S. (2015). Relating fuel loads to overstorey structure and composition in a fire-excluded Sierra Nevada mixed conifer forest. *International Journal of Wildland Fire, 24*(4), 484–494.
Lydersen, J., & North, M. (2012). Topographic variation in structure of mixed-conifer forests under an active-fire regime. *Ecosystems, 15*(7), 1134–1146.
Maltamo, M., Eerikainen, K., Pitkanen, J., Hyyppa, J., & Vehmas, M. (2004). Estimation of timber volume and stem density based on scanning laser altimetry and expected tree size distribution functions. *Remote Sensing of Environment, 90*, 319–330.
McLane, A. J., McDermid, G. J., & Wulder, M. A. (2009). Processing discrete-return profiling LiDAR data to estimate canopy closure for large-area forest mapping and management. *Canadian Journal of Remote Sensing, 35*, 217–229.
Mongus, D., & Zalik, B. (2014). Computationally efficient method for the generation of a digital terrain model from airborne LiDAR data using connected operators. *IEEE Journal of Selected Topics in Applied Earth Observations and Remote Sensing, 7*(1), 340–351.
Moore, M. M., Huffman, D. W., Fulé, P. Z., Covington, W. W., & Crouse, J. E. (2004). Comparison of historical and contemporary forest structure and composition on permanent plots in southwestern ponderosa pine forests. *Forest Science, 50*(2), 162–176.
Muldavin, E., & Tonne, P. (2003). *A vegetation survey and preliminary ecological assessment of Valles Caldera National Preserve.* New Mexico. Albuquerque, NM, USA: Natural Heritage.
Mutlu, M., Popescu, S. C., Stripling, C., & Spencer, T. (2008). Mapping surface fuel models using LiDAR and multispectral data fusion for fire behavior. *Remote Sensing of Environment, 112*(1), 274–285.
Nelson, R., Krabill, W., & MacLean, G. (1984). Determining forest canopy characteristics using airborne laser data. *Remote Sensing of Environment, 15*(3), 201–212.
Ouzts, J., Kolb, T., Huffman, D., & Meador, A. S. (2015). Post-fire ponderosa pine regeneration with and without planting in Arizona and New Mexico. *Forest Ecology and Management, 354*, 281–290.
Pascual, C., Garcia-Abril, A., Cohen, W. B., & Martin-Fernandez, S. (2010). Relationship between LiDAR-derived forest canopy height and Landsat images. *International Journal of Remote Sensing, 31*(5), 1261–1280.
Pereira, L. G., & Janssen, L. L. F. (1999). Suitability of laser data for DTM generation: A case study in the context of road planning and design. *ISPRS Journal of Photogrammetry and Remote Sensing, 54*(4), 244–253.
Popescu, S. C., Wynne, R. H., & Scrivani, J. A. (2004). Fusion of small-footprint LiDAR and multispectral data to estimate plot-level volume and biomass in deciduous and pine forests in Virginia, USA. *Forest Science, 50*(4), 551–565.
Renslow, M., Greenfield, P., & Guay, T. (2000). *Evaluation of multi-return LiDAR for forestry applications. RSAC-2060/4810-LSP-0001-RPT1.* US Department of Agriculture Forest Service - Remote Sensing Applications Center.
Reutebuch, S. E., McGaughey, R. J., Andersen, H. E., & Carson, W. W. (2003). Accuracy of a high-resolution LiDAR terrain model under a conifer forest canopy. *Canadian Journal of Remote Sensing, 29*(5), 527–535.
Reynolds, R. T., Sánchez Meador, A. J., Youtz, J. A., Nicolet, T., Matonis, M. S., Jackson, P. L., et al. (2013). *Restoring composition and structure in Southwestern frequent-fire forests.* USDA Forest Service-General Technical Report RMRS-GTR (310 RMRS-GTR).

Roberts, S. D., Dean, T. J., Evans, D. L., McCombs, J. W., Harrington, R. L., & Glass, P. A. (2005). Estimating individual tree leaf area in loblolly pine plantations using LiDAR-derived measurements of height and crown dimensions. *Forest Ecology and Management, 213*(1), 54–70.

Rogan, J., & Yool, S. R. (2001). Mapping fire-induced vegetation depletion in the Peloncillo Mountains, Arizona and New Mexico. *International Journal of Remote Sensing, 22*(16), 3101–3121.

Ryan, K. C., Knapp, E. E., & Varner, J. M. (2013). Prescribed fire in north American forests and woodlands: History, current practice, and challenges. *Frontiers in Ecology and the Environment, 11*(1), 15–24.

Sasaki, T., Imanishi, J., Ioki, K., Morimoto, Y., & Kitada, K. (2012). Object-based classification of land cover and tree species by integrating airborne LiDAR and high spatial resolution imagery data. *Landscape and Ecological Engineering, 8*(2), 157–171.

Scholl, A. E., & Taylor, A. H. (2010). Fire regimes, forest change, and self-organization in an old-growth mixed-conifer forest, Yosemite National Park, USA. *Ecological Applications, 20*(2), 362–380.

Sivanpillai, R., Smith, C. T., Srinivasan, R., Messina, M. G., & Wu, X. B. (2006). Estimation of managed loblolly pine stand age and density with Landsat ETM+ data. *Forest Ecology and Management, 223*(1), 247–254.

Smith, A. M., Falkowski, M. J., Hudak, A. T., Evans, J. S., Robinson, A. P., & Steele, C. M. (2009). A cross-comparison of field, spectral, and LiDAR estimates of forest canopy cover. *Canadian Journal of Remote Sensing, 35*(5), 447–459.

Spanner, M. A., Pierce, L. L., Peterson, D. L., & Running, S. W. (1990). Remote sensing of temperate coniferous forest leaf area index: The influence of canopy closure, understory vegetation and background reflectance. *Remote Sensing, 11*(1), 95–111.

Stephens, S. L., Agee, J. K., Fulé, P. Z., North, M. P., Romme, W. H., Swetnam, T. W., et al. (2013). Managing forests and fire in changing climates. *Science, 342*(6154), 41–42.

Stephens, S. L., Collins, B. M., & Roller, G. (2012). Fuel treatment longevity in a Sierra Nevada mixed conifer forest. *Forest Ecology and Management, 285*, 204–212.

Stevens, J. T., Safford, H. D., & Latimer, A. M. (2014). Wildfire-contingent effects of fuel treatments can promote ecological resilience in seasonally dry conifer forests. *Canadian Journal of Forest Research, 44*(8), 843–854.

Stevens, J. T., Safford, H. D., North, M. P., Fried, J. S., Gray, A. N., Brown, P. M., et al. (2016). Average stand age from forest inventory plots does not describe historical fire regimes in ponderosa pine and mixed-conifer forests of western North America. *PLoS One, 11*(5), e0147688.

Suárez, J. C., Ontiveros, C., Smith, S., & Snape, S. (2005). Use of airborne LiDAR and aerial photography in the estimation of individual tree heights in forestry. *Computers & Geosciences, 31*(2), 253–262.

Tucker, C. J. (1979). Red and photographic infrared linear combinations for monitoring vegetation. *Remote Sensing of Environment, 8*(2), 127–150.

Vogelmann, J. E., Howard, S. M., Yang, L., Larson, C. R., Wylie, B. K., & Van Driel, J. N. (2001). Completion of the 1990's National land cover data set for the conterminous United States. *Photogrammetric Engineering & Remote Sensing, 67*, 650–662.

Vogelmann, J. E., Tolk, B., & Zhu, Z. (2009). Monitoring forest changes in the southwestern United States using multitemporal Landsat data. *Remote Sensing of Environment, 113*(8), 1739–1748.

Wing, B. M., Ritchie, M. W., Boston, K., Cohen, W. B., Gitelman, A., & Olsen, M. J. (2012). Prediction of understory vegetation cover with airborne LiDAR in an interior ponderosa pine forest. *Remote Sensing of Environment, 124*, 730–741.

Wulder, M. A., White, J. C., Alvarez, F., Han, T., Rogan, J., & Hawkes, B. (2009). Characterizing boreal forest wildfire with multi-temporal Landsat and LIDAR data. *Remote Sensing of Environment, 113*(7), 1540–1555.

Xian, G., Homer, C., & Fry, J. (2009). Updating the 2001 National Land Cover Database land cover classification to 2006 by using Landsat imagery change detection methods. *Remote Sensing of Environment, 113*(6), 1133–1147.

Xu, H. (2006). Modification of normalised difference water index (NDWI) to enhance open water features in remotely sensed imagery. *International Journal of Remote Sensing, 27*(14), 3025–3033.